Tribology International 190 (2023) 109019

Contents lists available at ScienceDirect

Tribology International

journal homepage: www.elsevier.com/locate/triboint

Effect of the shape and size of interfacial micro-cavities on the adhesion of elastic solids

Elena Pierro [a], Giuseppe Carbone [b,c,*]

[a] School of Engineering, University of Basilicata, 85100 Potenza, Italy
[b] Department of Mechanics, Mathematics and Management, Polytechnic University of Bari, V.le Japigia, 182, 70126, Bari, Italy
[c] Physics Department M. Merlin, CNR Institute for Photonics and Nanotechnologies U.O.S. Bari, via Amendola 173, Bari, 70126, Italy

ARTICLE INFO

Keywords:
Contact mechanics
Adhesion
Dimple arrays
Cavity array
Suction effect
Bio-inspired adhesive

ABSTRACT

Microstructuring surfaces may strongly affect the adhesive behaviour at the contact interface, resulting in enhanced or weakened adhesion depending on the geometry of the surface structures and material properties. In this study we investigate the effects of size, shape and geometrical distribution of micro-cavities on the adhesion between an elastic solid and a rigid substrate. We show that reducing the lattice size by keeping constant the cavity size, may significantly weak the adhesion strength of the interface as a consequence of the interaction of the elastic stress and deformation fields generated by each single microcavity.

1. Introduction

The design of reversible surfaces is a research topic that has been dealt with very intensively in recent years [1–5], but it still requires a lot of in-depth analyses in the context of adhesive performance between elastic solids. Switchable adhesives in contact mechanics, indeed, play a crucial role in many practical applications, ranging from robotics [6,7] to biomedics [8,9]. In nature, so many examples have been observed that have inspired researchers. One of the most popular case study is the tokay-gecko, which is able to efficiently modulate the interfacial adhesion and grip leading to unparallelled climbing abilities [10,11]. Most of the studies presented so far, have mainly dealt with the improvement of adhesive performance of solids, through the optimization of the morphological properties of the contact surfaces [12]. In this view, both theoretical and experimental analyzes have been carried out to find solutions to enhance the adhesive pull-off force. Among such solutions we recall: (i) micro-patterned surfaces [13–15], (ii) optimized micro-fibrillars geometries [16,17], or (iii) specifically tuned material viscoelastic properties mimicking biomaterials already existing in nature [18–21]. All these studies have proved the feasibility of effective methods to tune the pull-off force needed to debond an elastic solid from a rigid substrate. However, how strong adhesion can be switched to low adhesion and easen the contact release has not been fully addressed yet and requires additional investigations — see Ref. [22] for a thorough collection of the state of the art on this topic. Among the proposed methods for tuning the interaction between two surfaces, we find electrically [23–25], thermally [26] or magnetically [27] - controlled adhesion. Most recently researchers have investigated the possibility to surface micro-cavities to generate micro-suction effects and tailor the adhesive properties of contacting surfaces. By adding micro-cups on the contact area [28], or by realizing micro-dimples on the substrate surface [29,30], it is possible to adjust the gas pressure entrapped in such voids, so to enhance the adhesion or to quickly suppress the grip, depending on the specific contact stage. Many experiments on texturized substrates, have shown that the amount of gas inside these prefabricated rigid bubbles is the key factor for effective adhesion at a given time. So far, the main efforts have been devoted in understanding the best shape of the gas volume geometry at the interface [31], e.g. cylindrical or hemispherical [32], the proper number of micro-cavities [33,34], and their possible periodic distribution on the surface [32,35].

Most of the studies found in literature are numerical ones, which makes it rather difficult identify the crucial parameters controlling multiple defect propagation at the interface and, in turn, adhesion. In the present paper we make an attempt to shed light on phenomena affecting adhesive performance of an elastic flat punch in contact with a rigid substrate, in presence of both a single hemispherical cavity and a periodic array of cavities with same shape. Starting from an accurate analytical model previously presented by the authors [36], where the effects on adhesion due the presence of a bubble of gas at the interface between a mushroom shaped micro-pillar and a rigid substrate have been deeply analysed, we now point out our attention

* Corresponding author at: Department of Mechanics, Mathematics and Management, Polytechnic University of Bari, V.le Japigia, 182, 70126, Bari, Italy.
E-mail address: carbone@poliba.it (G. Carbone).

https://doi.org/10.1016/j.triboint.2023.109019
Received 1 January 2023; Received in revised form 5 October 2023; Accepted 9 October 2023
Available online 12 October 2023

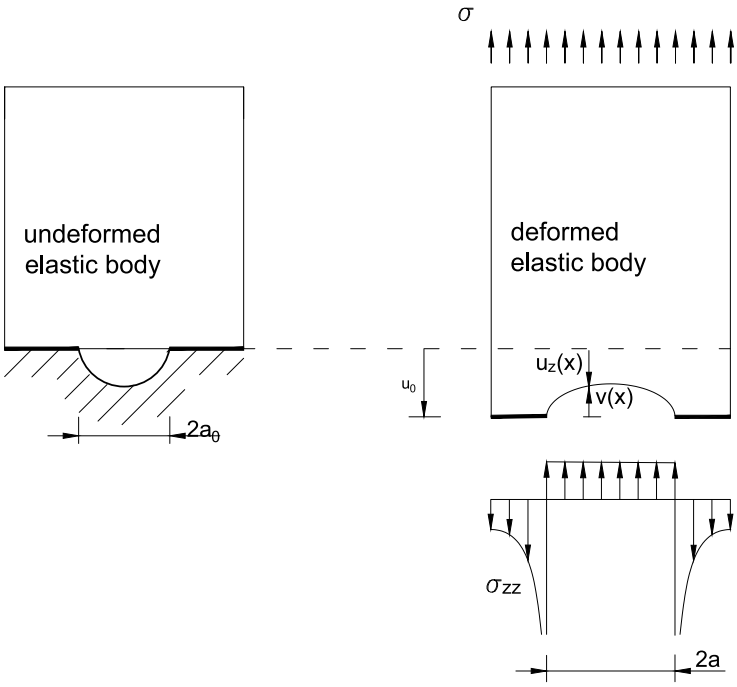

Fig. 1. The elastic punch in contact with a rigid substrate, in presence of a semi-spherical cavity, with radius a_0, and with air inside at $p = p_{atm}$ (a); the interfacial stress distribution, when a uniform external load σ is applied (b).

to what happens when the voids are placed on the rigid counterpart of the contact interface, and investigate the effect on adhesion of the geometry of the cavity, as well as the influence of the initial air pressure inside the void. Then we extend the investigation to the case of an array of cavities and examine how the pull-off stress is also affected by the lattice constant of the square array of cavities. The effect of cavity interspacing originates from the interaction between the elastic stress and strain field originated by each single crack. This will lead to a change of the stress intensity factors along the perimeter of the cavities as showed in Ref. [37] for the case of a periodic array of coplanar penny-shaped cracks.

2. Single cavity

Let us consider the elastic flat punch shown in Fig. 1, in contact with a rigid substrate, which presents a hemispherical cavity of radius a_0 and volume $V_0 = 2/3\pi a_0^3$, with a certain amount of gas entrapped inside. With the aim of calculating the pull off force required to detach the elastic pillar from the rigid substrate, we follow the thermodynamical approach previously proposed by the authors [36] , where the solution of the contact is obtained by minimizing the total energy stored at the interface as a consequence of local interfacial deformations [38]. To carry out the calculation we assume that the radius a_0 of the cavity is much smaller than the diameter and the height of the pillar, enabling us to consider the pillar as an elastic half-space in contact with a rigid substrate. We define the total Helmholtz free interfacial energy $\mathcal{F}$ [36,38] as

$$\mathcal{F}(V,a) = \mathcal{E}(V,a) + U_G(V) + U_A(a) \tag{1}$$

being $\mathcal{E} = (p+\sigma)V/2$ the interfacial elastic energy, $V = \int v(\mathbf{x})\, d^2x$ is the contribution to the volume of the void at the interface [Fig. 1(b)] due to the gap distribution $v(\mathbf{x}) = u_0 - u(\mathbf{x})$ at the interface, where u_0 is the total displacement and $u(\mathbf{x})$ is the elastic displacement distribution, σ is the external applied stress, p is the air pressure inside the cavity. The adhesion energy is $U_A(a) = \pi a^2 \Delta\gamma$, with $\Delta\gamma$ being the Duprè energy of adhesion and πa^2 the detached area, whereas $U_A(V)$ is the free energy of the entrapped gas under isothermal conditions. We assume that the entrapped gas satisfy the ideal gas law $pV = nRT$, being n the number of moles, R the ideal gas constant and T the absolute temperature. Under these conditions, the free energy of the gas can be calculated as $U_G(V) = -nRT \ln\left[\left(V+V_0\right)/V_0\right]$. Moreover, linear elasticity yields $V = \kappa\ (\sigma + p)$, being $\kappa = 8a^3/(3E^*)$ [36,39], $E^* = E/\left(1-\nu^2\right)$, ν the Poisson's ratio and E the Young's modulus.

In our analysis, we keep constant the asymptotic load σ so that the volume V of the void changes as the radius a of the contact area is changed. Therefore, for constant asymptotic load the proper thermodynamic potential is the interfacial Gibbs energy $\mathcal{G}(\sigma,a)$ that is obtained by taking the Legendre transform of the Helmholtz free energy $\mathcal{F}(V,a)$ (see Appendix A in Ref. [36]), i.e.

$$\mathcal{G}(\sigma,a) = \mathcal{F}(V,a) - \left.\frac{\partial \mathcal{F}}{\partial V}\right|_a V \tag{2}$$

which leads to

$$\mathcal{G}(\sigma,a) = \frac{1}{2}(p-\sigma)V - nRT\ln\frac{V+V_0}{V_0} + \pi a^2\Delta\gamma \tag{3}$$

We note that in order to increase the suction effect and augment the ability of the pillars to remain attached to the substrate, a compressive preload is often applied [Fig. 2-(b)] which causes part of the entrapped gas to leak out of the cavity. This is equivalent to reduce the number of moles n entrapped in the cavity, or, recalling that $p_0V_0 = nRT$, to modify the reference gas pressure $p_0 = nRT/V_0$. The more the pillar is pushed towards the rigid substrate, the lower is the reference pressure p_0.

In order to find the equilibrium state of the system we must require that $\partial\mathcal{G}(\sigma,a)/\partial a|_\sigma = 0$, which is the closure equation leading to the value of $a = a_{eq}$ at the equilibrium. Of course, because of the presence of the hemispherical cavity of radius a_0 and volume $V_0 = 2\pi a_0^3/3$, solutions with $a_{eq} < a_0$ are not physically meaningful as the contact void cannot have a radius smaller than a_0. In such a case $a = a_0$ is a stable equilibrium solution provided that $\partial\mathcal{G}(\sigma,a)/\partial a|_{\sigma,a_0} > 0$. For $a_{eq} \geq a_0$ the equilibrium stability requires $\partial^2\mathcal{G}(\sigma,a)/\partial a^2\Big|_{\sigma,a_{eq}} > 0$. For stable contacts the load σ can be supported by the system, however as soon as $\partial^2\mathcal{G}(\sigma,a)/\partial a^2\Big|_{\sigma,a_{eq}} = 0$ the equilibrium becomes unstable and the load cannot be supported any longer, we name this critical load as the pull-off stress σ_{cr}. To find the equilibrium solution, we need to

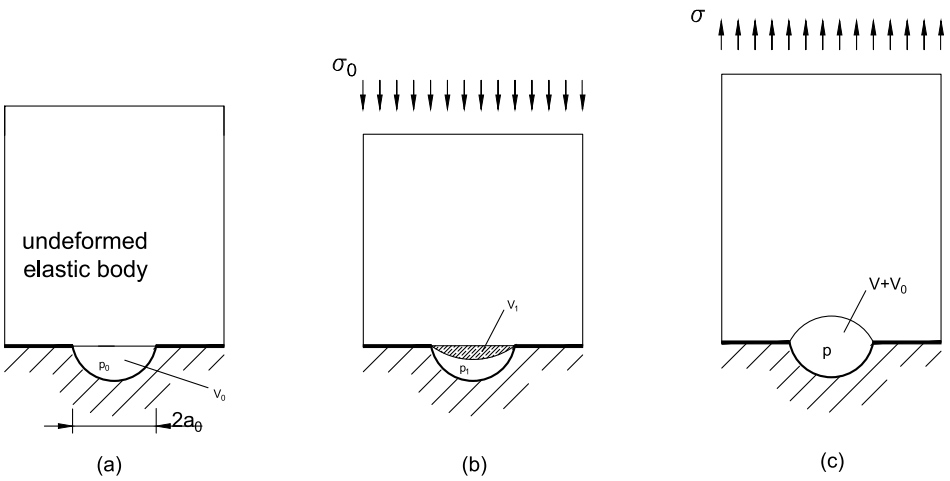

Fig. 2. The elastic punch in contact with a rigid substrate, in presence of a semi-spherical cavity, with radius a_0 (a); the interfacial deformation, due to the compressive preload, make the air volume reduced to $V_0 - V_1$, and the pressure inside the cavity equal to p_1 (b); the volume of the entrapped air $V + V_0$ corresponding to an external uniform tractive stress σ (c).

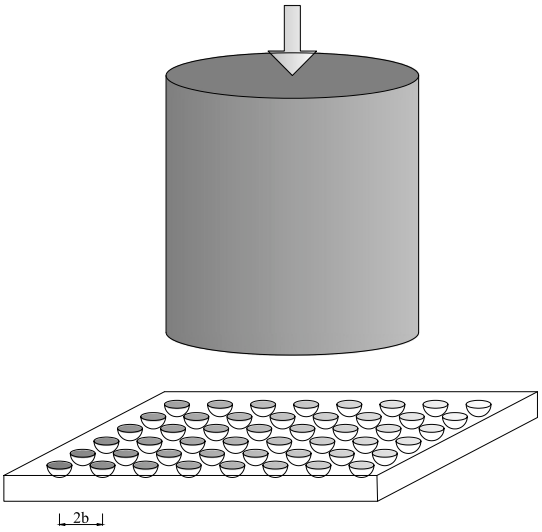

Fig. 3. The elastic flat punch approached towards the rigid substrate, which presents a periodic distribution of hemispherical dimples, of radius a_0 and periodicity $2b$.

write $\mathcal{G}(\sigma, a)$ as a function of σ and a only. To this end, we recall that $pV = p_0 V_0 = nRT$ and that $V = \kappa\ (\sigma + p)$, with $\kappa = 8a^3/(3E^*)$. Solving these two equations for V and p we get

$$p(\sigma, a) = \frac{1}{2}\left(-\sigma + \sqrt{\sigma^2 + \pi p_0 E^* \frac{a_0^3}{a^3}}\right) \tag{4}$$

and

$$V(\sigma, a) = \frac{4}{3}\frac{a^3}{E^*}\left(\sigma + \sqrt{\sigma^2 + \pi p_0 E^* \frac{a_0^3}{a^3}}\right) \tag{5}$$

which then give

$$\mathcal{G}(\sigma, a) = -\frac{2}{3}\frac{a^3}{E^*}\left(\sigma^2 + \sigma\sqrt{\sigma^2 + \pi p_0 E^* \frac{a_0^3}{a^3}} - \frac{\pi}{2} p_0 E^* \frac{a_0^3}{a^3}\right) - \frac{2}{3}\pi p_0 a_0^3 \ln\left[1 + \frac{2}{\pi}\frac{a^3}{a_0^3}\frac{1}{E^*}\left(\sigma + \sqrt{\sigma^2 + \pi p_0 E^* \frac{a_0^3}{a^3}}\right)\right] + \pi a^2 \Delta\gamma \tag{6}$$

3. Periodic array of interacting cavities

Now let us consider the case of a square-lattice of periodic distribution of hemispherical defects at the interface with spatial period (or lattice constant) $2b$ and area $A_0 = 4b^2$ (Fig. 3). In this case the problem can be formulated as done in Sec. 2 for the case of the single defect at the interface. However, this time the constant of proportionality κ_P appearing in the linear relation $V = \kappa_P(\sigma + p)$, where $V = \int_{A_0} v(\mathbf{x})\, d^2x$ will differ from κ because of the elastic interaction among the different square cells. We show in Appendix that κ_P can be calculated if one knows the stress intensity factor distribution along the boundary of the defect as a function of the linear size of the defect. Indeed we show that

$$\kappa_P(A) = -2\frac{U(\sigma, A)}{\sigma^2} = \frac{1}{\sigma^2 E^*}\int_0^1 d\zeta\zeta \int_0^{2\pi} d\theta r^2(\theta)\, K_I^2[\zeta r(\theta), \theta] \tag{7}$$

In what follows we assume that the detached area can be well approximated by a circle of radius a. This approximation is very accurate provided that a is sufficiently smaller than the lattice constant b. For larger value of a the approximation is less accurate, but except for a factor of order unity, the specific shape of the detached area do not change the qualitative physical behaviour of the system. So let as assume $r(\theta) = a$ independent of θ so Eq. (7) reads

$$\kappa_P(a) = \frac{2\pi}{\sigma^2 E^*}\int_0^a d\rho\rho \bar{K}_I^2(\rho) \tag{8}$$

where we have defined the average square value $\bar{K}_I^2(\rho) = (2\pi)^{-1}\int_0^{2\pi} K_I^2(\rho, \theta)\, d\theta$.

The stress intensity factor $K_I(a, b, \theta)$ is given for the case of a square lattice of penny shaped crack in Ref. [37]

$$K_I(a, b, \theta) = K_I^0 h\left(\frac{a}{b}, \theta\right) \tag{9}$$

where θ is the angular position of the generic point along the circular crack, and $K_I^0 = 2\sigma\sqrt{a/\pi}$ is the stress intensity factor for an interfacial single penny shaped crack. Once the quantity $\kappa_P(A)$ is calculated, it is possible to proceed to the evaluation of the energy $\mathcal{G}(\sigma, a)$ following exactly the same argument reported in Sec. 2, see Eqs. (3) –(6), and determine the pull-off stress σ_{cr} required to cause detachment.

4. Dimensionless formulation

The equations presented above can be reformulated in a dimensionless form, through the introduction of the following quantities $\tilde{\sigma} = \sigma/E^*$, $\tilde{p} = p/E^*$, $\tilde{a} = a/\delta$, $\tilde{b} = b/\delta$, $\tilde{V} = V/\delta^3$, being $\delta = \Delta\gamma/E^*$ the

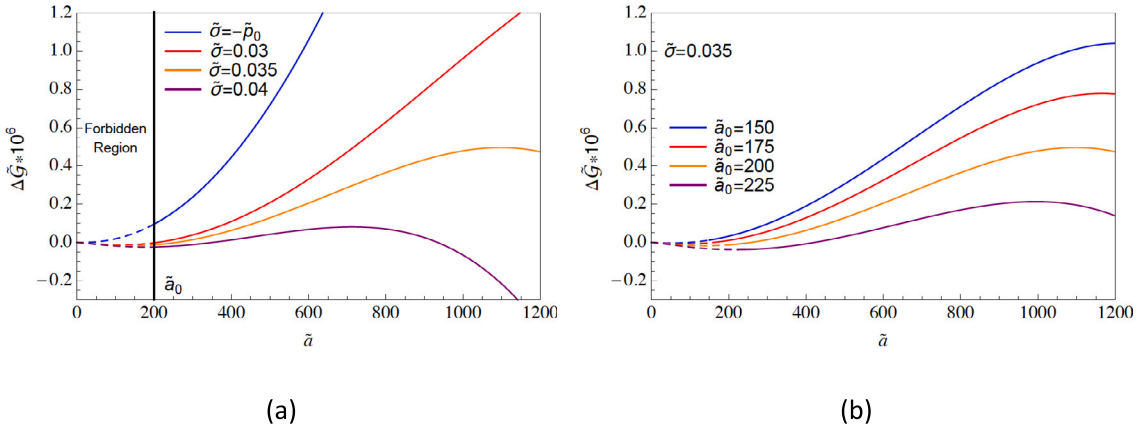

Fig. 4. The total energy variation $\Delta\tilde{\mathcal{G}}$ in the case of a single cavity at the interface, for $\tilde{a}_0 = 200$, and different values of the external applied stress $\tilde{\sigma}$ (a), and for a fixed load $\tilde{\sigma} = 0.042$, considering different sizes of the hemispherical dimple (b). In both the cases, the dashed lines indicate the areas with $\tilde{a}_{eq} < \tilde{a}_0$, which has no physical significance.

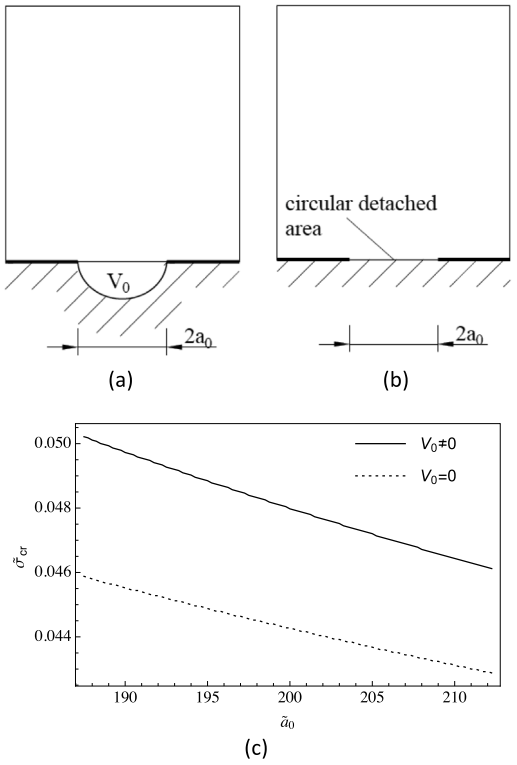

Fig. 5. The elastic pillar in contact with the rigid substrate, with a pre-existing volume V_0 of air at the interface of the rigid substrate (a), and with a circular detached area (b). The critical stress $\tilde{\sigma}_{cr}$ is shown as a function of the radius $\tilde{a}_0$, in presence of an initial volume of air V_0 (solid line), and for a circular detached area with $V_0 = 0$ (dotted line) (c).

adhesion length. In this way, the dimensionless interfacial Gibbs energy becomes

$$\tilde{\mathcal{G}}(\tilde{\sigma},\tilde{a}) = \frac{\mathcal{G}}{\delta^3 E^*} = -\frac{2}{3}\tilde{a}^3\left(\tilde{\sigma}^2 + \tilde{\sigma}\sqrt{\tilde{\sigma}^2 + \pi\tilde{p}_0\frac{\tilde{a}_0{}^3}{\tilde{a}^3}} - \frac{\pi}{2}\tilde{p}_0\frac{\tilde{a}_0{}^3}{\tilde{a}^3}\right) - \frac{2}{3}\pi\tilde{p}_0\tilde{a}_0{}^3\ln\left[1 + \frac{2}{\pi}\frac{\tilde{a}^3}{\tilde{a}_0{}^3}\left(\tilde{\sigma} + \sqrt{\tilde{\sigma}^2 + \pi\tilde{p}_0\frac{\tilde{a}_0{}^3}{\tilde{a}^3}}\right)\right] + \pi\tilde{a}^2 \tag{10}$$

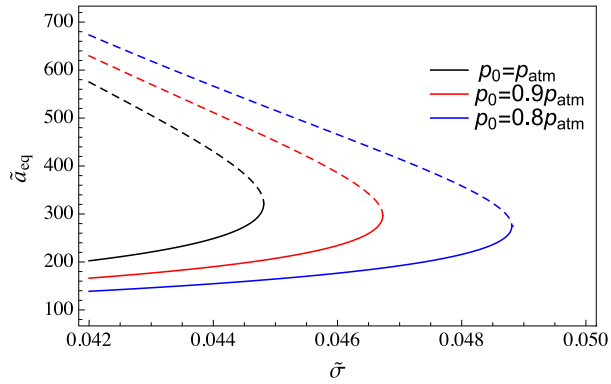

Fig. 6. The stable (dashed upper branch) and unstable (solid lower branch) equilibrium states $\tilde{a}_{eq}$, as functions of the applied stress $\tilde{\sigma}$, for different values of the pressure p_0 inside the cavity of volume V_0, corresponding to different compressive pre-loads, and for $\tilde{a}_0 = 200$. The condition $p_0 = p_{atm}$ corresponds to zero pre-load.

5. Results

In this Section we present the results of our analysis, aimed at understanding how the presence of an initial volume in the rigid substrate, both in a single cavity and in a distribution of interacting cavities, can contribute to the overall adhesive performance of an elastic flat punch. In our calculations, we assume $E^* = 4\text{MPa}$, $\Delta\gamma = 16\text{mJ/m}^2$ and $p_{atm} = 1\text{bar}$, having defined the asymptotic applied stress as $\sigma = \sigma_0 - p_{atm}$. The first case under analysis is when only one dimple is present at the interface, and no compressive pre-load is applied. In Fig. 4-(a), the corresponding total energy variation, defined as $\Delta\tilde{\mathcal{G}}(\tilde{\sigma},\tilde{a}) = \tilde{\mathcal{G}}(\tilde{\sigma},\tilde{a}) - \tilde{\mathcal{G}}(\tilde{\sigma},0)$, is shown as a function of the radius $\tilde{a}$ of the detached area, for $\tilde{a}_0 = 200$ and for four different values of the external applied stress $\tilde{\sigma}$. The forbidden region is related to solutions which have $\tilde{a}_{eq} < \tilde{a}_0$, which are not physically meaningful as previously explained. For an unloaded pillar [see the solid line for $\tilde{\sigma} = -p_0$ in Fig. 4-(a)], only the stable equilibrium state is present, corresponding to the minimum of the curve. Notice that, by increasing the external applied stress, the energy barrier, defined as the difference between the energy values at the two equilibrium states, decreases. In a similar way, at fixed tractive load $\tilde{\sigma}$, the energy barrier of the system decreases for greater values of $\tilde{a}_0$, as shown in Fig. 4-(b). However, the presence of the gas in the hemispherical volume V_0 at the interface of the rigid substrate [Fig. 5 - (a)], changes the behaviour of the system compared to the sole presence

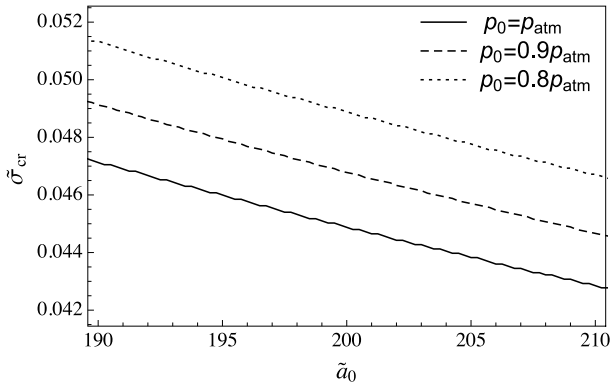

Fig. 7. The critical stress $\tilde{\sigma}_{cr}$ as a function of the radius $\tilde{a}_0$, for different values of the pressure p_0 inside the cavity of volume V_0, corresponding to different compressive pre-loads. It is evident the stabilizing effect due to lower values of p_0.

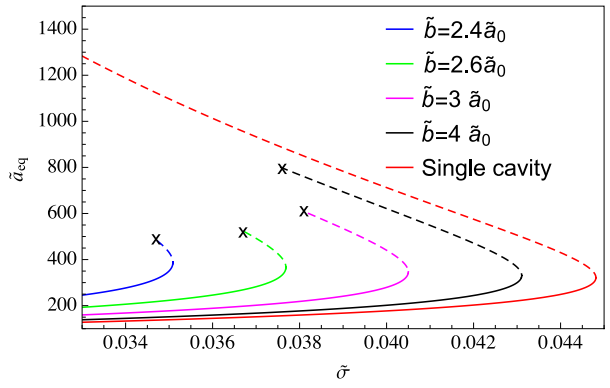

Fig. 8. The stable and unstable equilibrium values $\tilde{a}_{eq}$ as functions of the external applied stress $\tilde{\sigma}$, for different wavelengths of the cavity array $\tilde{b}$, and for $\tilde{a}_0 = 200$. The cross represents, for every line, the value beyond which $\tilde{a}_{eq}$ cannot increase, as it exceeds the dimension $\tilde{b}$.

of a circular detached area of radius $\tilde{a}_0$ [Fig. 5-(b)], as studied by the authors in Ref. [36]. In particular, a sort of stabilizing effect is observed, i.e. given the same values of the radius $\tilde{a}_0$, the energy barrier increases when a pre-existing air volume V_0 is present at the interface. This is clearly shown in Fig. 5-(c), where the critical stress $\tilde{\sigma}_{cr}$ is plotted vs. the radius $\tilde{a}_0$ in the two cases. When an initial volume V_0 of gas is present at the interface, the required stress to detach the pillar from the substrate is always greater, independently of the radius $\tilde{a}_0$. Nevertheless, in both the cases, by increasing the radius $\tilde{a}_0$, the critical stress $\tilde{\sigma}_{cr}$ tends to drop, and this happens because of the energy barrier decreases [Fig. 4 -(b)]. As mentioned so far, in order to increase the resistance of the pillar in separating from the substrate, usually a compressive preload is applied to the system [Fig. 2-(b)], which determines the leakage of a certain amount of gas from the cavity, ad a consequent reduction of number of moles n of entrapped gas or equivalently of the reference cavity pressure p_0, [Fig. 2-(c)]. The more the pillar is pushed towards the rigid substrate, the lower is the reference pressure p_0 inside the cavity. In Fig. 6, the stable and unstable equilibrium states $\tilde{a}_{eq}$ of the system are shown versus the remote applied stress $\tilde{\sigma}$. The upper branch is the unstable equilibrium and the lower branch is the stable one. Results are shown for three different values of the initial air pressure p_0, and for $\tilde{a}_0 = 200$. It is possible to observe that when a compressive pre-load is applied to the pillar, i.e. by decreasing p_0, the critical stress $\tilde{\sigma}_{cr}$, which is the intersection point of the two equilibrium states, tends to raise. This result can be more easily observed in Fig. 7, where the critical stress $\tilde{\sigma}_{cr}$ is plotted for increasing values of the radius $\tilde{a}_0$, for three different values of the pressure p_0. By increasing the dimension of the cavity, i.e. for higher values of $\tilde{a}_0$, the stress required to detach the pillar from the substrate becomes smaller, however, given the presence of the volume V_0 at the interface, it is possible to rise the adhesive performance of the pillar in terms of $\tilde{\sigma}_{cr}$ by applying a pre-compression, as shown in Fig. 7 for smaller values of p_0.

It is now interesting to evaluate the pillar resistance to the detachment, when an array of cavities is present at the interface. In this perspective, we consider a rigid substrate with a square distribution of hemispherical voids with period $2\tilde{b}$ (Fig. 3). We first compare the single cavity considered so far, with the adhesive behaviour of one cell of the periodic array, with dimensions $2\tilde{b} \times 2\tilde{b}$. In Fig. 8, it is possible to observe that by increasing the number of the cavities, at fixed radius $\tilde{a}_0 = 200$, i.e. when the wavelength $2\tilde{b}$ decreases, the stress needed to detach the single cell from the substrate, found as intersection between the stable and the unstable branches, becomes smaller. Fig. 9 shows the critical stress $\tilde{\sigma}_{cr}$ as a function of the radius $\tilde{a}_0$, for different values of the periodicity $2\tilde{b}$. In particular, the greater is the wavelength $2\tilde{b}$, the more the curves tend to move towards the red line, which represents the single cavity case. This behaviour is expected,

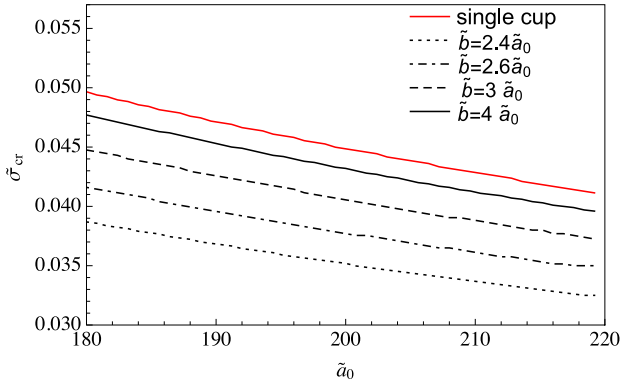

Fig. 9. The critical stress $\tilde{\sigma}_{cr}$ as a function of $\tilde{a}_0$, for different values of $\tilde{b}$. Also the single cavity case is shown (red curve). By increasing the periodicity $2\tilde{b}$, the adhesive behaviour of the cell is similar to the one of a single cavity.

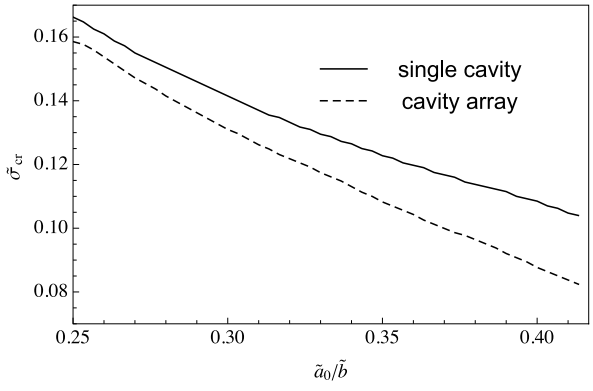

Fig. 10. The critical stress $\tilde{\sigma}_{cr}$ as a function of $\tilde{a}_0/\tilde{b}$, for $\tilde{a}_0 = 150$. For increasing values of the ratio $\tilde{a}_0/\tilde{b}$, the adhesive performance of the pillar drops when an array of cavities is present at the interface, with respect to the single cavity case.

since the larger the lattice spacing, the more the stress intensity factor of the periodic array tends to coincide to the equivalent value of a single cavity [37]. On the contrary, when the cavities are approached, i.e. when $2\tilde{b}$ decreases, their interaction becomes very significant and the stress intensity factor increases, so that the detachment of the cell takes place at smaller loads. In Fig. 10 the critical stress $\tilde{\sigma}_{cr}$ is shown as a function of $\tilde{a}_0/\tilde{b}$, for a fixed radius $\tilde{a}_0 = 150$. For low values of the ratio $\tilde{a}_0/\tilde{b}$, there is no appreciable difference between the two cases. However, by decreasing the distance between the cavities, i.e. by

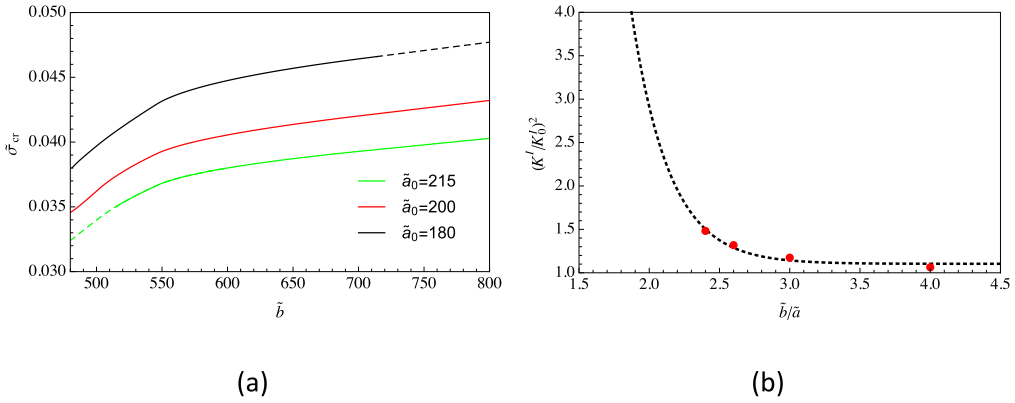

Fig. 11. The critical stress $\tilde{\sigma}_{cr}$ as a function of the half distance $\tilde{b}$ between the cavities, for different values of $\tilde{a}_0$. Dashed lines have been calculated by considering the extrapolation of the average square stress intensity factor $\left(\bar{K}_I/K_I^0\right)^2$ (a). The extrapolation of $\left(\bar{K}_I/K_I^0\right)^2$ is shown vs. $\tilde{b}/\tilde{a}$ (dashed line), together with the values given in Ref. [37] (red points) (b).

increasing the ratio $\tilde{a}_0/\tilde{b}$, the critical stress $\tilde{\sigma}_{cr}$ tends to decrease when an array distribution is considered. Even more clearly, in Fig. 11-(a), the critical stress $\tilde{\sigma}_{cr}$ is plotted vs. $\tilde{b}$, for different values of $\tilde{a}_0$. The dashed lines have been obtained by extrapolation of the average square values $\left(\bar{K}_I/K_I^0\right)^2$, shown in Fig. 11 -(b) (dashed line), since the stress intensity factor (see Eq. (9)) is provided in Ref. [37] only in four points $\tilde{b}/\tilde{a} = \{2.4; 2.6; 3; 4\}$ (red points in Fig. 11-(b)). In all the cases shown in Fig. 11-(a), the critical stress $\tilde{\sigma}_{cr}$ raises by increasing the gap between the cavities, up to an almost constant value, which coincides with that corresponding to the single cavity.

In conclusion, the enhancement of the adhesion between an elastic pillar and a rigid substrate by means of an array of micro-cavities at the interface, increases by decreasing the air reference pressure within the cavities but it is strongly affected by the interaction of the elastic fields generated by each single cavity. The proposed analytical approach enables the evaluation of both the optimal distance and the correct dimension of the cavities, and allows us to conclude that in order to get benefits in using a distribution of cavities, it is convenient to keep the ratio $\tilde{b}/\tilde{a}$ sufficiently high. This, together with the initial precompression would improve the adhesive performance of the elastic solids.

6. Conclusions

In this work we presented a theoretical study to assess the adhesive performance of structured surfaces covered with a distribution of micro hemispherical cavities. At first, we considered a single cavity, whose adhesive strength was compared with the case of a simple circular detached area at the interface, of same radius and zero volume. The presence of a micro-void determines a suction effect, very often exploited in the contact mechanics, because of its beneficial contribute to the pull-off stress. Additionally, we evaluated the effect of a compressive pre-load on the adhesion performance. By assuming that a certain amount of gas is squeezed out from the interface, a stronger suction effect is observed, thus resulting in the rising of the critical stress beyond which the surface detaches. In this perspective, the effect on adhesion of a periodic distribution of hemispherical cavities was also considered. Our results show that when the size of the cavity is small compared to the lattice constant, the pull-off stress does not change significantly compared to the case of the single cavity. However, increasing the radius of the cavities at fixed lattice constant, the interaction of elastic fields generated by the cavities penalizes the adhesive mechanisms and reduces the pull-off stress. Our study may help engineers to properly tune the strength of adhesion by controlling the number and size of interfacial micro-voids and the preload at the interface.

Declaration of competing interest

The authors declare that they have no known competing financial interests or personal relationships that could have appeared to influence the work reported in this paper.

G. C. thanks the Italian Ministry of Education, University and Research(Programme “Department of Excellence” Legge 232/2016”) and the European Union NextGenerationEU (National Sustainable Mobility Center CN00000023, Italian Ministry of University and Research Decree n. 1033—17/06/2022, Spoke 11–Innovative Materials & Lightweighting).

Data availability

Data will be made available on request.

Appendix. The calculation of the void compliance κ from the stress intensity factors K_I

In this section we show how one can calculate the elastic compliance of the void moving from the knowledge of the stress intensity factors along the border of the cavity, for cavity size varying from zero to the actual value. Recall that linear elasticity allows us to state, for any given shape (non necessarily circular) of the detached area of size (maximum diameter) $2a$, that $V = \kappa_P(\sigma + p)$ this time with $\kappa_P \neq \kappa$. We needs to calculate $\kappa_P(A)$ which depends on the specific geometry of the void and on the fact that the system is periodic or not. Since $\kappa_P(A)$ does not depend on the load σ or on the presence of gas pressure p inside the cavity, we will carry out our argument assuming $p = 0$ (i.e. no gas entrapped at the interface). We only assume the presence of a constant remote stress σ acting on the system. In this case the energy release rate is defined as $G = -\partial U/\partial A|_\sigma$ where the total energy U (sum of the interfacial elastic energy $\mathcal{E}$ and mechanical energy associate with the load σ) is simply given by the Legendre transform of the interfacial elastic energy $\mathcal{E} = \sigma V/2 = V^2/(2\kappa_P)$, i.e.

$$U(\sigma, A) = \mathcal{E} - \left.\frac{\partial \mathcal{E}}{\partial V}\right|_A V = -\frac{1}{2}\sigma V = -\frac{1}{2}\kappa_P \sigma^2 \tag{A.1}$$

Therefore, from the definition of the energy release rate, one can write, under the condition of constant remote stress σ

$$dU|_\sigma = -G dA = \frac{1}{2}\sigma^2 d\kappa_P \tag{A.2}$$

which connects the energy release rate to the change of the compliance κ_P as the contact area has changed of the infinitesimal quantity dA. To calculate the potential energy $U(\sigma, A)$, which only depends on the

actual configuration of the system, we can choose any reversible transformation which, under constant load σ, modifies the detached area from zero to the actual value A. To this end a convenient transformation is a scaling transformation that keeps unchanged the shape of the area as it increase from zero to A. Under a scaling transformation the radial coordinate of any point of the boundary can be expressed as $\rho(\theta,\zeta) = \zeta r(\theta)$ where $r(\theta)$ is the shape function i.e. the function describing the boundary of the actual area A in polar coordinates, and ζ the scaling factor varying over the interval $0 \leq \zeta \leq 1$. The local change of the contact area can be then phrased as $dA = \rho d\rho d\theta = r^2(\theta)\ \zeta d\zeta d\theta$ and the change of the total energy U writes

$$dU|_\sigma = -G(\rho,\theta)\,\rho d\rho d\theta = -G[\zeta r(\theta),\theta]\,r^2(\theta)\ \zeta d\zeta d\theta \tag{A.3}$$

recalling that for $\zeta = 0$ the interfacial total energy vanishes, performing a double integration yields

$$U(\sigma,A) = -\int_0^1 d\zeta\zeta \int_0^{2\pi} d\theta r^2(\theta)\, G[\zeta r(\theta),\theta] \tag{A.4}$$

Recalling that within the framework of linear fracture mechanics, $G = K_I^2/(2E^*)$ we also get

$$U(\sigma,A) = -\frac{1}{2E^*}\int_0^1 d\zeta\zeta \int_0^{2\pi} d\theta r^2(\theta)\, K_I^2[\zeta r(\theta),\theta] \tag{A.5}$$

so that the compliance κ_P can be finally calculated as

$$\kappa_P(A) = -2\frac{U(\sigma,A)}{\sigma^2} = \frac{1}{\sigma^2 E^*}\int_0^1 d\zeta\zeta \int_0^{2\pi} d\theta r^2(\theta)\, K_I^2[\zeta r(\theta),\theta] \tag{A.6}$$

As an example consider the case of an isolated interfacial penny shaped crack, in such a case the stress intensity factor is

$$K_I^0 = 2\sigma\sqrt{\frac{\rho}{\pi}} = 2\sigma\sqrt{\frac{\zeta a}{\pi}} \tag{A.7}$$

so by replacing we get

$$\kappa = -2\frac{U(\sigma,A)}{\sigma^2} = \frac{8a^3}{3E^*} \tag{A.8}$$

which is the correct value for a penny shaped crack.

References

[1] Lee H, Lee BP, Messersmith PB. A reversible wet/dry adhesive inspired by mussels and geckos. Nature 2007;448(7151):338–41.

[2] Chen S, Gao H. Bio-inspired mechanics of reversible adhesion: Orientation-dependent adhesion strength for non-slipping adhesive contact with transversely isotropic elastic materials. J Mech Phys Solids 2007;5(55):1001–15.

[3] Wu J, Kim S, Chen W, Carlson A, Hwang KC, Huang Y, et al. Mechanics of reversible adhesion. Soft Matter 2011;18.

[4] Zhao Y, Wu Y, Wang L, Zhang M, Chen X, Liu M, et al. Bio-inspired reversible underwater adhesive. Nature Commun 2017;8(2218).

[5] Johannes K, Calahan K, Bowen L, Zuetell E, Long R, Rentschler M. Mechanically switchable micro-patterned adhesive for soft material applications. Extreme Mech Lett 2022;52(101622).

[6] Tang Y, Zhang Q, Lin G, Yin J. Switchable adhesion actuator for amphibious climbing soft robot. Soft Robotics 2018;5(5):592–600.

[7] Yang M, Cooper LP, Liu N, Wang X, Fok MP. Twining plant inspired pneumatic soft robotic spiral gripper with a fiber optic twisting sensor. Opt Express 2020;28(23):35158–67.

[8] Xianga T, Houa J, Xiea H, Liu X, Gonga T, Zhoua S. Biomimetic micro/nano structures for biomedical applications. Nanotoday 2020;35(100980).

[9] Bowen LK, Johannes K, Zuetell E, Calahan KN, Edmundowicz SA, Longa R, et al. Patterned enteroscopy balloon design factors influence tissue anchoring. J Mech Behav Biomed Mater 2020;111(103966).

[10] Autumn K, Liang YA, Hsieh ST, Zesch W, Chan WP, Kenny TW, et al. Adhesive force of a single gecko foot-hgas. Nature 2000;405:681–5.

[11] Gao H, Wang X, Yao H, Gorb S, Arzt E. Mechanics of hierarchical adhesion structures of gecko. Mech Mater 2005;37:275–85.

[12] Tian H, Li X, Shao J, Wang C, Wang Y, Tian Y, et al. Gecko-effect inspired soft gripper with high and switchable adhesion for rough surfaces. Adv Mater Interfaces 2019;1900875.

[13] Shahsavan H, Zhao B. Conformal adhesion enhancement on biomimetic microstructured surfaces. Langmiur 2011;27(12):7732–42.

[14] Tang T, Hui CY, Glassmaker NJ. Can a fibrillar interface be stronger and tougher than a non-fibrillar one? J R Soc Interface 2005;2(5):505–16.

[15] Im HS, Kim JU, Han S, Kim T-i. Process, design and materials for unidirectionally tilted polymeric micro/nanohgass and their adhesion characteristics. Polymers 2016;8(326).

[16] Carbone G, Pierro E. Origin of the superior adhesive performance of mushroom-shaped microstructured surfaces. Soft Matter 2011;7(12):5545–52.

[17] Carbone G, Pierro E. Sticky bio-inspired micropillars: Finding the best shape. Small 2012;8(9):1449–54.

[18] Pierro E, Afferrante L, Carbone G. Tuning the mechanical properties of the viscoelastic materials, for the improvement of their adhesive performance. In: Abdel Wahab M, editor. Proceedings of the 9th international conference on fracture, fatigue and wear. Lecture notes in mechanical engineering, Singapore: Springer; 2022, 2021.

[19] Pierro E, Afferrante L, Carbone G. On the peeling of elastic tapes from viscoelastic substrates: Designing materials for ultratough peeling. Tribol Int 2020;146:106060.

[20] Pierro E, Carbone G. A new technique for the characterization of viscoelastic materials: Theory, experiments and comparison with DMA. J Sound Vib 2021;515(10):116462.

[21] Pierro E. Damping control in viscoelastic beam dynamics. J Vib Control 2020;26(19–20):1753–64.

[22] Liu Z, Yan F. Switchable adhesion: On-demand bonding and debonding. Adv Sci 2022;2200264.

[23] Mastrangelo M, Caruso F, Carbone G, Cacucciolo V. Electroadhesion zipping with soft grippers on curved objects. Extreme Mech Lett 2023;101999. http://dx.doi.org/10.1016/j.eml.2023.101999.

[24] Cacucciolo V, Shea H, Carbone G. Peeling in electroadhesion soft grippers. Extreme Mech Lett 2022;50:101529. http://dx.doi.org/10.1016/j.eml.2021.101529.

[25] Cantini E, Wang X, Koelsch P, Preece JA, Ma J, Mendes PM. Electrically responsive surfaces: Experimental and theoretical investigations. Acc Chem Res 2016;49(6):1223–31.

[26] Ye Z, Lum GZ, Song S, Rich S, Sitti M. Phase change of gallium enables highly reversible and switchable adhesion. Adv Mater 2016;28(25):5088–92.

[27] Wang S, Luo H, Linghu C, Song J. Elastic energy storage enabled magnetically actuated, octopus-inspired smart adhesive. Adv Funct Mater 2021;31(9).

[28] Huang R, Zhang X, Li W, Shang L, Wang H, Zhao Y. Suction cups-inspired adhesive patch with TailorablePatterns for versatile wound healing. Adv Sci 2021;8(2100201).

[29] Qiao S, Wang L, Jeong H, Rodin GJ, Lu N. Suction effects in cratered surfaces. J R Soc Interface 2017;14.

[30] Roy T, Choudhurya D, Mamat AB, Murphya BP. Fabrication andcharacterizationofmicro-dimplearrayonAl_2O_3 surfaces byusingamicro-tooling. Ceram Int 2014;40:2381–8.

[31] Akerboom S, Appel J, Labonte D, Federle W, Sprakel J, Kamperman M. Enhanced adhesion of bioinspired nanopatterned elastomers via colloidal surface assembly. Interface 2014;12:20141061.

[32] Wang L, Ha K-H, Qiao S, Lu N. Suction effects of crater arrays. Extreme Mech Lett 2019;30:100496.

[33] Dai Q, Chang Q, Li M, Huang W, Wang X. Non-sticky and non-slippery biomimetic patterned surfaces. J Bionic Eng 2020;17:326–34.

[34] Nannia G, Fragoulia D, Ceseracciu L, Athanassiou A. Adhesion of elastomeric surfaces structured with micro-dimples. Appl Surf Sci 2015;326:45–150.

[35] Zheng S, Liu Q, He J, Wang X, Ye K, Wang X, et al. Critical adhesion areas of cells on micro-nanopatterns. Nano Res 2022;15(2):1623–35.

[36] Carbone G, Pierro E. Effect of interfacial gas entrapment on the adhesion of bioinspired mushroom-shaped micro-pillars. Soft Matter 2012;8(30).

[37] Sekine H, Mura T. Weakening of an elastic solid by a periodic array of penny-shaped cracks. Int J Solids Struct 1979;15:493–502.

[38] Carbone G, Mangialardi L. Analysis of the adhesive contact of confined layers by using a Green's function approach. J Mech Phys Solids 2008;56(2):684–706.

[39] Maugis D. Contact, adhesion and rupture of elastic Solids. Springer series in solid state sciences, Berlin, Heidlberg, New-York: Springer-Verlag; 1999.